




Burning Rate of Wood Cribs with Controlled Airflow

S. McAllister * and T. Grumstrup, RMRS Missoula Fire Sciences Laboratory, USDA Forest Service, 5775 W US Highway 10, Missoula, MT 59808, USA

Received: 24 March 2023/**Accepted:** 10 July 2023/**Published online:** 16 August 2023

Abstract. There is a dire need to improve our prediction capabilities of wildland fire behavior in a range of conditions from marginal burning to the most extreme. In order to develop a more physically-based operational wildland fire behavior model, we need to improve our understanding of the effect of ventilation on burning rate of fuel beds. In this work, wood cribs are used as a simplified fuel bed. A variety of crib designs were tested with stick sizes ranging from 0.32 cm to 1.27 cm and porosities ranging from densely packed to loosely packed. A pressurized box was built that allowed for a controlled flow rate of air through the cribs from 100 LPM to 1000 LPM. The mass loss rates with forced ventilation were compared to tests conducted outside of the box under unrestricted quiescent conditions. For the flow rates tested here, the burning rate was generally observed to increase with flow. The amount of air naturally induced into a crib while burning was deduced to be best related to the vent area and the square root of the stick spacing ($A_v s^{1/2}$). It was seen that the air-to-fuel ratio inside a fuel bed burning in quiescent conditions is approximately 1.11, indicating that over 75% of the air required to completely combust the pyrolysis gases is entrained in the plume. When the supplied air is less than the amount normally entrained in ambient burning, the crib is under-ventilated and the proportional reduction in the burning rate does not seem to depend on the crib characteristics. When the crib is over-ventilated, however, the relative increase in the burning rate does vary with crib design. Simple physical arguments were used to correlate the data. Future work will include testing at higher flow rates, different moisture contents, and with cribs built with multiple stick thicknesses.

Keywords: Burning rate, Wood cribs, Ventilation, Wildland fire

Abbreviations

A_v	Area of the vertical shafts in the crib (cm^2) ($A_v = s^2(n - 1)^2$)
A_s	Exposed surface area of the sticks (cm^2)
b	Stick thickness (cm)
c_p	Specific heat of ambient air (kJ/kg-K)
g	Acceleration due to gravity (m/s^2)
h	Crib height (cm)
Δh_c	Heat of combustion (kJ/g)
l	Stick/crib length (m)

*Correspondence should be addressed to: S. McAllister, E-mail: sara.mcallister@usda.gov



\dot{m}_a	Forced air flow rate (g/s)
\dot{m}_b	Burning rate (g/s)
n	Number of sticks per layer ()
N	Number of layers ()
\dot{Q}	Heat release rate (kW)
Q^*	Non-dimensional heat release rate ()
s	Spacing between sticks (cm)
T_∞	Ambient air temperature (K)
ϕ	Crib porosity (cm) as defined in Equation 1 or [16]
ρ_∞	Ambient air density (g/cm ³ or kg/m ³)

1. Introduction

Wildfires are increasingly impacting society, injuring and killing people, burning down structures, and/or choking large areas with heavy toxic smoke. To better prepare for and mitigate against the worst of the impacts, accurate fire behavior models are necessary. Current operational wildland fire models in the United States take a semi-empirical approach to fire spread predictions [1–3], while many other systems around the world employ strictly empirical predictions of spread rate (for example [4] and [5]). These models have limited accuracy in both extreme and marginal conditions [6, 7]. Examples of extreme fire behavior not captured by operational models include fire-atmospheric interactions or “plume dominated” fire, vorticity-driven spread such as fire whirls or vorticity-driven lateral spread, or mass fires [6]. Examples on the marginal end include highly discontinuous fuels, high fuel moisture contents, and other considerations important for conducting prescribed fires [7]. These limits in our current operational models create an urgent need for new predictive tools for both prescribed burning and wildfire management [7]. The development of a new operational fire behavior model is underway to fill this need [8]. Because fire spread consists of complex interactions between burning, airflow, heat transfer, and ignition processes, the wildfire spread model incorporates all these processes within the context of a spreading fire [8]. By understanding the whole fire spread cycle, this model will be able to predict not just spread rates, but will answer other very important questions like whether a fire will even spread or not. However, there are many details about the underlying processes of wildland fire spread that are not well understood [9]. One area where understanding is lacking is the burning rate and residence time of a porous fuel bed, especially as ventilation is increased, as with a wind. This work is intended to answer how airflow influences burning rates of porous fuel beds, such as in wildland fires.

Wildland fuels are extremely complex, with large possible variations in fuel element sizes, shapes, and arrangements, as well as variation in chemical composition over the course of the growing season and between different vegetation species, making it difficult to gain traction on the problem of understanding the different mechanisms controlling their burning behavior. Naturally occurring fuel beds, such as pine needle beds or individual trees themselves, will always have some variability in the arrangement of the fuels that is uncontrollable. A simplified fuel bed is thus needed, such as wood cribs (ordered cross-piles of single-sized wood

sticks). Wood crib fires have already played a major role in the development of wildland fire spread models in use. The Rothermel model [1], which is the basis of all operational wildfire tools in the U.S. and elsewhere, was developed using cribs with 0.64 and 1.27 cm (1/4" and 1/2") sticks as well as pine needles and excelsior. Flame heights in crown fires in U.S. wildfire behavior models are estimated using a relation from Thomas developed using crib fire experiments [10]. Others such as Fons, Anderson, and Byram have also sought to understand wildland fires using wood cribs [11–13]. Much other work has been done with cribs, particularly for compartment fire behavior applications, with Gross, Block, and Heskestad providing the foundational papers [14–16]. Gross established that two regimes exist: a densely-packed regime where the ventilation is limited and the burning rate increases with increasing porosity; and a loosely-packed regime where the burning rate is more governed by heat and mass transfer processes of the individual sticks [14]. Block provided the first theoretical analysis of the two regimes [15], while Heskestad [16] re-correlated the data of Gross [14] and Block [15] to generate perhaps the most well-used description of the porosity (ϕ , cm):

$$\frac{\dot{m}_b}{A_s b^{-1/2}} = fn(\phi) = fn\left[\left(\frac{A_v}{A_s}\right) s^{1/2} b^{1/2}\right] \tag{1}$$

where \dot{m}_b is the burning rate (g/s), A_s is the exposed surface area of the sticks (cm^2), b is the stick thickness (cm), A_v (cm^2) is the area of the vertical shafts in the crib ($A_v = s^2(n - 1)^2$ where n is the number of sticks per layer), and s is the spacing between sticks (cm). This porosity factor is essentially an air-to-fuel ratio inside the fuel bed. Though not as well-used in the literature, the correlation by Thomas [17] was shown in [18] to be more accurate for cribs with thin elements and those that deviate greatly from the more standard cubic shapes of the early works:

$$\frac{\dot{m}_b}{A_s \rho_\infty (gh)^{0.5}} = 3.27 \frac{s}{h} \tag{2}$$

where ρ_∞ is the ambient air density (g/cm^3) and h is the crib height (cm).

Our basic understanding of wood cribs thus comes from studies conducted in ambient conditions (though the intended application of Heskestad’s and Thomas’s correlations was enclosure fires). Though many other studies exist that use cribs as fire sources in other contexts (such as tunnel fires [19] or firewhirls [20]), very few of them were undertaken to understand the behavior of the crib itself. Previous work in the literature has looked at the behavior in many aspects (for example [18, 21–24]), but have struggled to examine the true effect of increasing the ventilation within the fuel bed itself. For example, experiments conducted in the wind tunnel were hampered by flow effects where for certain crib geometries, the air would flow around the crib and not through [22]. By using a chimney in [24], flow through the crib was achieved, however, the flow was induced and therefore cou-

pled to the burning behavior, not completely controllable, and very difficult to measure.

The work by Harmathy [25] is one of the only that truly controls the flow through the crib. In this work, he used a sealed pressurized box to examine if the burning rate of cribs built from a variety of materials was sensitive to airflow. He found that the burning rate of cribs built from charring materials did indeed change with forced ventilation, but the burning rate of cribs built of non-charring materials did not. Here we replicate his apparatus and expand on his work to understand how the properties of the crib influence its response to ventilation. Previous work has also been unable to estimate the amount of air that is naturally induced through the fuel bed while burning in normal quiescent ambient conditions [24]. This paper attempts to answer several questions: Just how much air flows through the crib under unrestricted quiescent ambient conditions? What happens when that flow is reduced? What happens when that flow is increased? Do the characteristics of the crib change the behavior?

2. Experimental Methods

Cribs built from knot-free ponderosa pine wood are used as the fuel bed. Twelve crib designs were tested, as detailed in Table 1. The stick thickness ranged from 0.32 cm to 1.27 cm, and stick length from 12.7 cm to 30.48 cm. A range of porosities (as characterized by Heskestad, Equation 1 [16]) was tested from densely-packed to loosely-packed (see Figure 1). All cribs were dried in a conditioning chamber at 35°C and 3% RH for at least 3 days to attain an equilibrium moisture content of about 1%.

Table 1
Crib Designs Tested. Porosity was calculated using relation from Heskestad [16] (Equation 1). Cribs with porosity under about 0.05 cm are considered densely packed

Crib design #	Stick thickness (b, cm)	Stick length (ℓ , cm)	Number of sticks per layer (n, [])	Number of layers (N, [])	Exposed surface area (A_s , [cm ²])	Heskestad porosity (ϕ , cm)	Packing description ([])
1	1.27	12.7	5	10	2661.29	0.0215	Dense
2	1.27	20.3	6	14	7432.24	0.0390	Dense
3	1.27	25.4	4	21	10,077.40	0.1202	Loose
4	1.27	25.4	11	2	2519.35	0.0625	Transition
5	0.64	20.3	3	45	6757.25	0.1213	Loose
6	0.64	20.3	10	16	7177.41	0.0270	Dense
7	0.64	25.4	6	10	3658.06	0.2110	Loose
8	0.64	25.4	10	10	5806.44	0.0725	Transition
9	0.64	25.4	14	15	11,504.80	0.0213	Dense
10	0.64	30.5	8	14	8090.31	0.1210	Loose
11	0.32	25.4	14	30	12,487.10	0.0252	Dense
12	0.32	30.5	6	40	9055.63	0.1215	Loose



Figure 1. Example cribs. From left to right: densely-packed crib (crib design #9), transition (crib design #8), and loosely-packed crib (crib design #3).

The experimental apparatus consists of a 1.2 m \times 1.2 m pressurized box seen in Figure 2, similar to that initially used by [25]. The crib is placed on a 0.86 m by 0.86 m weighing platform consisting of a 3.2 mm-thick aluminum sheet with six sheets of 3.2 mm-thick ceramic paper insulation. The gap between the weighing platform and the box walls is sufficient to allow the air to flow in from the bottom and around the platform with minimal noise in the data. The crib sits on 7.62 cm steel risers which was shown in [18] to provide sufficient room for airflow underneath the crib (shorter risers resulted in reduced burning rates for the same crib designs tested here). The height of the lid is adjustable so that the top of the crib sits flush with the ventilation hole in the lid. A variety of inserts for the lid adjust the size of the ventilation hole to match the size of the crib being tested. The air flow rate through the crib is controlled by pressurizing the box with dry house air set by mass flow controllers. A rubber gasket on the base of the table ensures that the airflow must pass through the bottom and sides of the crib and out the ventilation hole at the top. As the volumetric flow through the crib can be controlled, conditions ranging from under-ventilated to over-ventilated can be tested. Airflow into the box was varied from 100 LPM to 1000 LPM (1.75 to 17.5 g/s assuming the elevation-adjusted air density is 1.05 kg/m³) for all crib designs, with higher flows prevented by house air capacity limitations. Note that only the volumetric flow rate through the crib is controlled, not the velocity of the air through the horizontal or vertical shafts. A set of experiments was also conducted outside of the box to establish the burning rate of each crib design in unrestricted, quiescent ambient conditions.



Figure 2. Left: Air box with lid up. Air enters the box through via PVC piping underneath the table. A rubber gasket prevents air from escaping downward from the box. Also seen are four adjustable supports that control the height of the lid. The weighing platform is covered in white ceramic paper insulation and sits on three (silver) load cells (one visible). Right: The lid is adjusted so that the top of the crib sits flush with the ventilation hole, ensuring that the airflow passes through the crib.

The burning rate is defined here as the change in mass of the solid fuel. The weight of the crib is recorded at 10 Hz using three 6-kg load cells, calibrated to 0.01%, contained within the box (Figure 2). Contact between the load cells and weighing platform is via ball bearings to minimize heat conduction to the load cells. The cribs were ignited by briefly dunking them in 99% pure isopropyl alcohol and allowing them to drain so that the amount of alcohol used was less than 10% of the crib weight. This alcohol was visually confirmed to burn off quickly and did not likely contribute to the reported peak burning rate results. Sufficient time between tests was given to allow the walls of the box to be cool to the touch. All test conditions were repeated at least three times (308 total tests) and the results averaged.

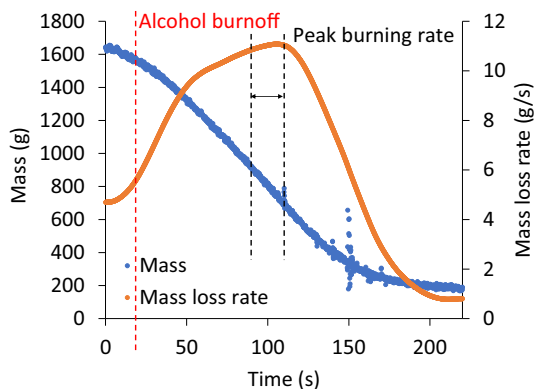


Figure 3. Raw mass data (blue) and mass loss rate (orange) for crib design #3 at 800 LPM. The alcohol used for ignition was visually seen to burn off in the first 15–20 s in this test, indicated by the red vertical dashed line. The region used to report the peak burning rate is marked by black vertical dashed lines. The noise at 150 s is due to the crib collapsing.

Figure 3 shows a sample of the raw mass data (blue). The orange line in Figure 3 is the continuous burning rate as measured as the mass loss rate. The continuous burning rate is calculated as the numerical derivative of the mass data using a spline fit with ten degrees of freedom to smooth out the noise in the data from numerical derivation, as well as from experimental sources like the ignition of the alcohol vapors and the collapse of the crib (seen in Figure 3 at 150 s). All tests followed the same temporal evolution of the burning rate, where the burning rate gradually increases to a maximum, then decreases until the visible flaming ceases. The reported burning rates are found by taking the slope of the best fit line through the mass data and are the maximum rates achieved during each experiment.

3. Results and Discussion

3.1. Burning Rate with Ventilation

Figure 4 shows the average peak burning rates for all crib designs as a function of the forced flow rate. The burning rates were normalized by the burning rate in unrestricted quiescent ambient conditions. The error bars indicate one standard deviation between replicate tests, which tended to increase with thinner sticks (and thus crib design number). This increased variability is possibly due to the increased numbers of sticks used per fuel bed, so variations in the dimensions and density of the sticks and how the beds were assembled compounded. More variability is also seen in most crib designs at 100 LPM, likely due to the somewhat marginal burning conditions. The average variability is 5.5% of the mean peak burning rate, and ranges from 0.63% to 23.12%. Given this mild variability, in

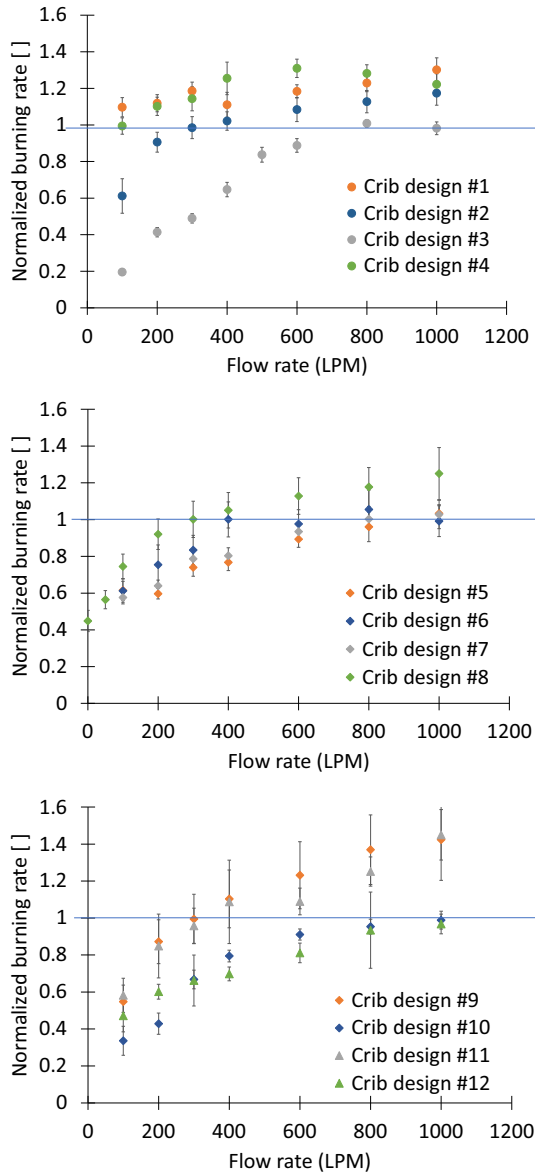


Figure 4. Variation with airflow of average peak burning rate normalized by the unrestricted quiescent value. Error bars indicate one standard deviation between replicate tests.

general, the burning rates are seen to increase with the air flow rate. There are two main reasons for this increase. For ventilation-limited cribs, an increase in the ventilation improves the air–fuel ratio, increasing the heat released and heat feedback to the solid fuels (for example [14, 15, 23]). This holds when the ventilation

is limited either because the cribs are densely packed or because of insufficient supplied airflow. Even if the cribs are not ventilation limited, increased airflow increases the char oxidation rate and therefore the mass loss rate of the solid fuel increases [25, 26].

There are some exceptions, however, to this increasing trend. For example, the apparent increasing trend for crib design #1 is very weak, as the measured peak burning rates are not statistically different from one another (p values > 0.05). An important note is even though they are not different from each other, the measured peak burning rates of crib design #1 at all flow rates except 400 LPM (which, for this crib design, had the largest experimental standard deviation of 5.4% of the mean) are statistically different from the unrestricted quiescent case.

An additional exception to the general monotonically increasing trend is the burning rate of crib design #4. For this case, the normalized burning rate decreased for flow rates above 600 LPM, indicating that the balance between heat release and heat losses had shifted. As the flow through the crib is increased, convective heat losses increase [27]. Additionally, the flames themselves get pushed upward, away from the solid fuel, likely reducing the heat feedback that contributes to the burning [23]. This non-monotonic behavior of the burning rate

Table 2
Crib Characteristics and the Estimated Entrained Airflow into the Crib During Peak Burning in Unrestricted Quiescent Ambient Conditions. Porosity was calculated using the relation from [16] (Equation 1). Cribs with porosity under about 0.05 cm are considered densely packed. The reported ambient burning rate is the average peak mass loss rate. The dimensionless heat release rate (Q^*) (Zukoski number) in unrestricted quiescent conditions is calculated from Equation 3. The estimated airflow into the crib is the amount of airflow required to match the unrestricted quiescent burning rate. The starred estimated air flow rates indicate those that occurred just outside of the tested flow rates

Crib design #	Stick thickness (b, cm)	Heskestad porosity (ϕ , cm)	Crib height (cm)	Ave initial crib mass (g)	Ambient burning rate (g/s)	Estimated Q^* (°)	Estimated air-flow into crib (LPM)
1	1.27	0.0215	12.70	434.9	1.92	4.17	100*
2	1.27	0.0390	17.78	1174.0	6.16	4.13	341
3	1.27	0.1202	26.67	1477.6	10.69	4.10	800
4	1.27	0.0625	2.54	401.7	2.66	1.02	105
5	0.64	0.1213	28.58	480.2	10.32	6.92	908
6	0.64	0.0270	10.16	596.8	6.82	4.57	400
7	0.64	0.2110	6.35	264.9	6.07	2.33	800
8	0.64	0.0725	6.35	483.9	7.00	2.68	300
9	0.64	0.0213	9.53	996.5	7.38	2.83	305
10	0.64	0.1210	8.89	610.2	12.35	3.00	1000*
11	0.32	0.0252	9.54	544.9	8.94	3.43	332
12	0.32	0.1215	12.72	369.3	16.95	4.12	1000*

with flow rate was also observed by Harmathy in [25] and in previous work using a chimney to induce flow through the crib [23]. Unfortunately, there is no one parameter that seems to characterize this “turning point.” For example, crib #8 has a similar porosity (see Table 2), but its burning rates still increases with air-flow in the range tested. The initial crib mass is another parameter that would be logical to suggest, but no relation with this parameter was found either. As seen from Table 2, crib designs #1, 5, 8, and 12 have similar initial masses, and crib design #7 weighs considerably less. The forced flow rate for crib #4 is about six times that naturally induced in normal ambient conditions (see discussion below in Sect. 3.2), but crib design #1 also had an equally low naturally induced flow with no clear decline in burning rate seen for the flows tested here. Crib design #1, however, is very dense (Table 1) so one could argue that its burning rate has more “potential” to increase with forced flow whereas crib design #4 is normally not ventilation limited. Crib design #4 is the shortest crib so the air inside the crib would likely have a lower temperature, providing more cooling to the stick surfaces, as well as the shortest residence time to participate in combustion. The non-dimensional heat release rate (Q^*), a.k.a. Zukoski number, could also be considered. Similar to the square root of the Froude number, the Zukoski number is frequently defined as [28]:

$$Q^* = \frac{\dot{Q}}{\rho_{\infty} c_p T_{\infty} g^{1/2} l^{5/2}} = \frac{\dot{m}_b \Delta h_c}{\rho_{\infty} c_p T_{\infty} g^{1/2} l^{5/2}} \quad (3)$$

where \dot{Q} is the heat release rate (kW), ρ_{∞} is the density of the ambient air (kg/m³), c_p is the specific heat of the ambient air (kJ/kg-K), T_{∞} is the ambient air temperature (K), g is the acceleration due to gravity (m/s²), l is the crib length (m), \dot{m}_b is the burning rate (g/s), and Δh_c is the heat of combustion (kJ/g). The heat of combustion is assumed to be 14.1 kJ/kg [29]. Since Q^* is related to the Froude number, smaller values would suggest that the momentum of the fuel gases exiting the fuel surface is very slow in unrestricted quiescent conditions, and a forced airflow would easily overwhelm this buoyant fuel flow. Crib design #4 has the lowest Q^* in unrestricted quiescent conditions (Table 2), but not drastically, so it is unclear what is driving this behavior without seeing at which flow rates the “turning points” occur for the other crib designs. Harmathy [25] saw this curvature explicitly for two of his crib designs (W-1-1 and W-1-2 is his notation). His Figure 5 is reproduced here in Figure 5. Unfortunately, a direct comparison to his data can’t really be made. In his setup, the cribs were placed on a screen directly on the liquid fuel ignition tray, effectively blocking off airflow from underneath the cribs. It was shown in [18] that placing the crib directly on the platform can reduce the burning rate by as much as 90% compared to when sufficient space is provided, such as was done in this work. Despite this, if one calculates the Q^* for his cribs using Equations 2 and 3 (for unrestricted ambient conditions), it would appear that the turning point for his cribs occurs at higher flow rates as Q^* increases (see Figure 5), suggesting that this parameter may indeed at least help explain this behavior.

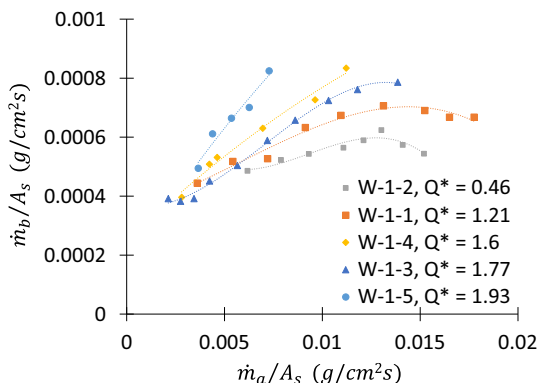


Figure 5. Variation in burning rate (\dot{m}_b , g/s) with forced air flow rate (\dot{m}_a , g/s) relative the surface area (A_s , cm^2). Data reproduced from Harmathy [25].

3.2. Induced Airflow in Unrestricted Conditions

In Figure 4, the burning rates have been normalized by the burning rates obtained in normal unrestricted quiescent conditions. Because the box is sealed with a finite and relatively limited initial supply of air that is likely largely consumed during ignition, normal entrainment of air into the fuel bed is suppressed during a large part of the burning duration. Consequently, when plotted as in Figure 4, the airflow that is naturally induced through the fuel bed can be inferred by finding the flowrate that corresponds to a normalized burning rate equal to one. Where necessary, linear interpolation was used when the match was achieved between two tested flow rates. For example, by re-examining Figure 4, we see that the normalized burning rate for crib design #6 is 1 (indicated by the horizontal blue line) when the flow is 400 LPM, thus the airflow induced in quiescent conditions is inferred to be 400 LPM. Similarly, using linear interpolation, the normalized burning rate for crib design #2 is 1 for a flow rate of 341 LPM. In some cases, this was not clearly achieved in the range of flow rates tested here. For example, crib design #1 appears to draw in less than 100 LPM of air into the fuel bed itself while burning in ambient conditions (at 100 LPM, the normalized burning rate was 1.10). On the other hand, crib designs #10 and 12 seem to pull in just over 1000 LPM into the fuel bed while burning in unrestricted quiescent conditions. At 1000 LPM, their normalized burning rates were 0.99 and 0.97, respectively. Unfortunately, testing at higher flows was limited by constraints on the house air supply, so the trends cannot be reliably extrapolated to confirm a more accurate estimate of the matched value. Because the normalized burning rates are very close to 1, a rough estimate of 1000 LPM seems like an acceptable first rough approximation. For flow rates less than 100 LPM, it was observed with crib design #8 that the outflow is so weak through the ventilation hole that there is a possibility that air can be pulled into the box from above. This results in much

higher uncertainty of what the flow actually is through the fuel bed, so no further testing at lower flow rates was conducted. Table 2 shows the values of the estimated naturally entrained flow rate into the body of the crib while burning at the peak rate in unrestricted quiescent conditions. Note that these are estimates of the amount of air only within the fuel bed and do not include the air that would be entrained into the fire and smoke plumes.

Intuitively, this air flow rate that is naturally entrained through the fuel bed under normal unrestricted quiescent ambient conditions generally increases with the burning rate. Figure 6 shows this estimated entrained flow into the crib as a function of the burning rate predicted by Thomas [17] from Equation 2. As mentioned earlier, the Thomas correlation [17] provides a better prediction of the burning rate for a wider variety of cribs than the Heskestad correlation [16] in Equation 1 [18]. This is confirmed here in Figure 7 which demonstrates agreement of the Thomas correlation with the experimental data to within 22%. The linear regression in Figure 6 suggests that the air-to-fuel ratio within in fuel bed is approximately 1.11. However, Quintiere and McCaffrey in [30] estimate that the stoichiometric air-to-fuel ratio for wood cribs is 4.92. By comparing these air-to-fuel ratios ($1.11/4.92 = 0.23$), it would seem then that the majority ($> 75\%$) of the air required to consume the pyrolyzed fuel is therefore entrained in the flame with only a small portion ($< 25\%$) passing through the fuel bed.

The path that the entrained flow takes through the crib was shown in [24] to be a complex problem where the resistances to flow in the horizontal and vertical directions are strongly dependent on the crib structure. In particular, as the aspect ratio (stick length divided by the stick thickness, l/b) of the crib increased, more and more of the airflow was shown to originate from below the crib. In [24], it is argued that for aspect ratios of 20 or larger ($l/b \geq 20$), such as for crib designs #3–12 tested here, limited airflow is likely through the sides. If inadequate space is provided below the crib, the burning rate will drop [18, 24], though it is unknown whether the entrained airflow through the horizontal sides of the crib will follow

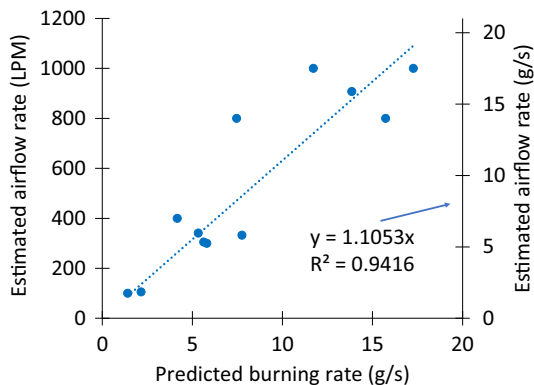


Figure 6. Estimated entrained air flow rate in unrestricted quiescent ambient conditions is related to the burning rate predicted by the Thomas correlation (Equation 2) [17].

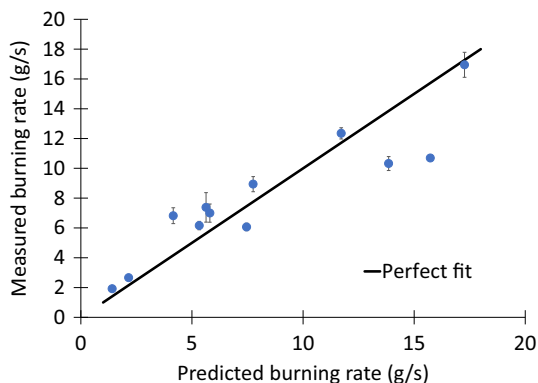


Figure 7. Comparison between the measured burning rates and those predicted with the Thomas correlation (Equation 2) [17]. Agreement is within 22%. Error bars indicate one standard deviation between replicate tests.

the same trend with the burning rate as reported here. It is possible that the suggested air–fuel ratio within the fuel bed is only applicable for cribs with unrestricted access to flow from underneath.

To define crib porosity as an air-to-fuel ratio, there have been at least two different methods of estimating the airflow through the crib. To develop his porosity factor, Heskestad estimated the air flow rate as $A_v s^{1/2}$ [16]. In [14] and [20], the volumetric buoyant airflow up through the crib vents was assumed to be related to $A_v h^{1/2}$. Figure 8 compares the experimentally determined air flow rates induced during unrestricted quiescent conditions to both relations from the literature. Interestingly, both relations correlated with the experimental values equally well and also as well as the predicted burning rate (Figure 6) (which is essentially $A_{s,s}/$

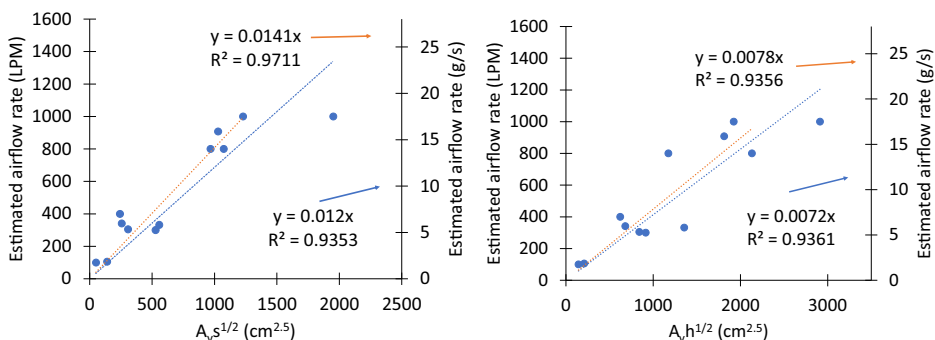


Figure 8. Experimentally estimated induced air flow rate during unrestricted quiescent burning compared to two relations from the literature to estimate airflow within cribs. Blue lines are fits to all crib designs and orange lines omit crib design # 12 (rightmost point).

$h^{1/2}$), at least based on the r^2 value. In [16], Heskestad argues that $A_{vs}^{1/2}$ fits the data better than $A_v h^{1/2}$, however, this is not clearly seen here. Though the r^2 value is about the same, the data visually look more scattered when $A_v h^{1/2}$ is used. However, if crib design #12 is omitted, which is the rightmost point in Figure 7 and likely had an induced air flow rate above the 1000 LPM assigned (see above discussion), the r^2 improves to 0.9711 for $A_{vs}^{1/2}$ but remains relatively unchanged at 0.9356 for $A_v h^{1/2}$ (orange lines in Figure 8). This suggests that $A_{vs}^{1/2}$ may indeed be a better term to use for the air flow rate as suggested by [16].

3.3. Normalized Burning and Air Flow Rates

Figure 9 replots the normalized burning rate, this time against the air flow rate normalized by the estimated entrained air flow rate in unrestricted quiescent conditions from Table 2. Figure 9 demonstrates that the data collapse to a single curve when the forced flow is below the naturally entrained flow (normalized flow rates below 1). In these “under-ventilated” conditions, the burning rate is clearly controlled by access to air only, and the relative reduction in the burning rate does not depend significantly on the characteristics of the fuel bed. This is seen more clearly in Figure 10 which zooms into the “under-ventilated” region to take a closer look, demonstrating an exponential increase up to unrestricted quiescent conditions. However, for “over-ventilated” conditions, the data do not collapse to a single curve, indicating that the fuel bed’s response to increased ventilation isn’t as straightforward, and the characteristics of the crib influence the relative increase in burning rate in this regime.

To understand how the fuel bed’s characteristics might influence the burning behavior in the “over-ventilated” regime, Figure 11 plots the data in a similar manner as Harmathy [25]. In this figure, the dimensioned burning rate (\dot{m}_b , g/s) and air flow rate (\dot{m}_a , g/s) are scaled by the exposed surface area of the sticks (A_s ,

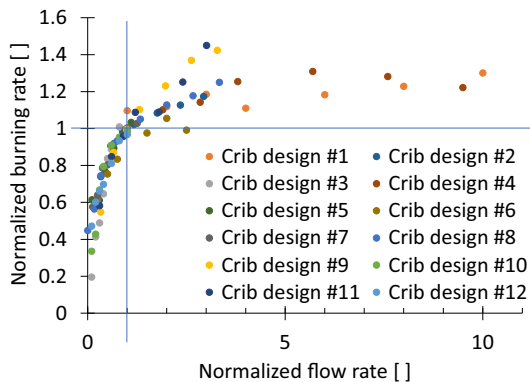


Figure 9. Normalized burning rate with normalized flow rate. Burning rate is normalized by the unrestricted quiescent burning rate. Flow rate is normalized by the estimated entrained air flow rate for burning in unrestricted quiescent conditions (see Table 2).

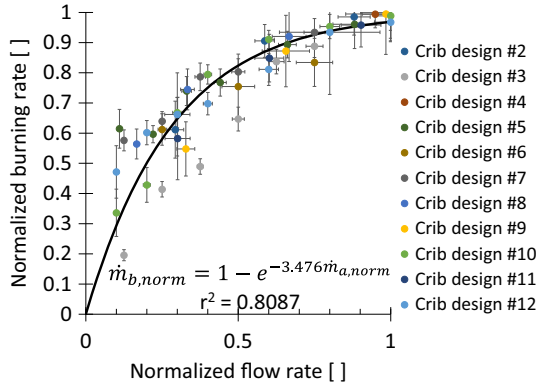


Figure 10. Normalized burning rate with normalized flow rate in the under-ventilated region. Burning rate is normalized by the measured unrestricted quiescent burning rate. Flow rate is normalized by the estimated entrained air flow rate for burning in unrestricted quiescent conditions (see Table 2). Error bars indicate one standard deviation.

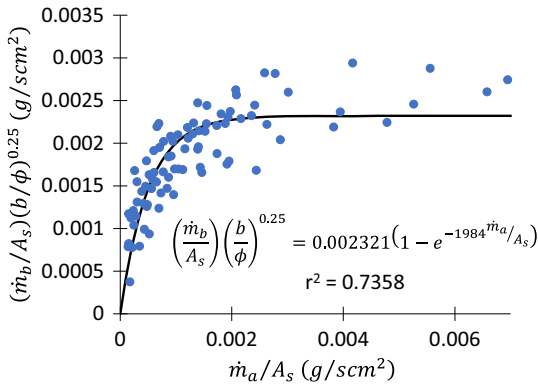


Figure 11. Burning rate (\dot{m}_b , g/s) with forced air flow rate (\dot{m}_a , g/s). Both axes have been scaled by the exposed surface area (A_s , cm^2), while the burning rate scaling also includes the stick thickness (b , cm) and porosity factor (ϕ , cm).

cm^2) (Table 1) so that both are in terms of a mass flux. Plotted this way, each crib design that Harmathy tested followed its own curve (as in Figure 5). However, in manipulating the data, it was noted that there is a slight dependence on the stick thickness (b , cm) and the crib porosity (ϕ , cm) as defined by Heskestad (Equation 1) [16]. By including these slight dependences and scaling the burning rate by the additional non-dimensional parameter $(b/\phi)^{0.25}$, all of the data appear to generally collapse to a single curve:

$$\left(\frac{\dot{m}_b}{A_s}\right)\left(\frac{b}{\phi}\right)^{0.25} = 0.002321\left(1 - e^{-1984\dot{m}_a A_s}\right) \tag{4}$$

In the literature [14–16], the burning rate is frequently scaled by $A_s b^{-0.5}$, as this is the “idealized” burning rate expected from an individual stick. The dependence on the stick thickness isn’t quite as strong here though (exponent of 0.25 instead of 0.5). The inclusion of the porosity factor (ϕ) is logical as it accounts for the natural air-to-fuel ratio of a particular crib. Dense cribs with a smaller porosity have more potential to increase their burning rate with forced flow. It is important to note that the x-axis in Figure 11 includes only the total exposed surface area, not how that surface area is arranged, hence the need for a parameter that describes the compactness of the fuel bed in the y-axis.

Returning to this notion of air-to-fuel ratios, Heskestad [16] correlated the burning rate normalized by the “idealized” value for an individual stick ($A_s b^{-0.5}$) as a function of the air-to-fuel ratio (ϕ , where the fuel quantity is also given by $A_s b^{-0.5}$). To pursue a similar approach, the “idealized” value of the burning rate for both axes is taken instead as the predicted quiescent burning rate (Equation 2 with constants inserted: $0.00119A_s \phi sh^{-0.5}$). Figure 12 shows the mass loss rate relative to this “idealized” value as a function of the ratio of the “forced” air-to-fuel ratio ($\dot{m}_a/0.00119A_s \phi sh^{-0.5}$) to the quiescent air-to-fuel ratio (ϕ). The x-axis is therefore an “equivalence ratio” of sorts. The line of best fit in Figure 12 is a slightly better fit to the data when treated this way (r^2 improved to 0.7990):

$$\frac{\dot{m}_b}{0.00119A_s \phi sh^{-0.5}} = 1.4864\left[1 - e^{-0.1013\frac{\dot{m}_a}{0.00119\phi A_s \phi sh^{-0.5}}}\right] \tag{5}$$

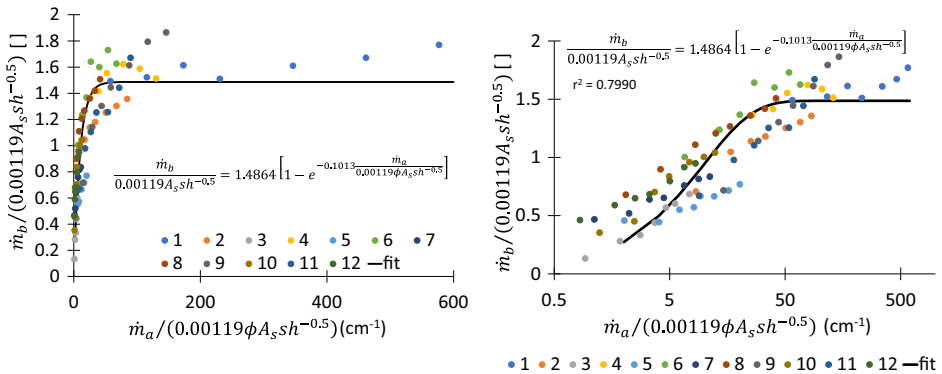


Figure 12. Dimensionless burning rates scaled by the predicted quiescent rate as a function of the “forced” air-to-fuel ratio to the quiescent air-to-fuel ratio. Left image is with standard axes, right is with a logarithmic x-axis to see the lower range more clearly. Each crib design is marked by different colors as indicated in the legends.

Note the general similarity of the shape of the curves in Figures 9, 10, 11 and 12 and form of Equations 4 and 5 to that found in Gross [14], Block [15], and Hestad [16] (for fit equation see [18]). This implies that there is a similar split into two regimes. When the airflow into the crib is small, the burning rate is controlled by the access to air. In this regime, the scaled burning rate (whether by $A_s(b/\phi)^{-0.25}$ or the quiescent burning rate) increases dramatically with airflow. At some point, the scaled burning rate begins to level off at some new “idealized” burning rate with further increases in airflow, before decreasing at high flow levels. Logically, this new “idealized” burning rate under forced flow would be sensitive to some parameter characterizing the crib’s denseness (ϕ , s , or A_v) and a parameter related to ability of air to promote char oxidization (A_s).

It is important to note that these lines are likely to curve downward for higher air flow rates as in Harmathy [25], so that this curve is only applicable over a certain range of airflows. However, for most crib designs, it was not possible to test sufficiently high flow rates here to observe this curvature, so it is still unknown exactly where this curvature occurs and what best predicts it. This is thus not accounted for in the approaches considered above. As mentioned earlier, unfortunately, a direct comparison to the data of Harmathy [25] where this curvature does occur can’t really be made because his setup likely reduced the airflow underneath the crib which could have a major influence on the resulting burning rate.

4. Conclusions and Future Work

In this work, a pressurized air box was built to examine the effect of the fuel bed characteristics on the burning rate in response to ventilation. For the flow rates tested here, the burning rate was generally observed to increase with flow. The following questions were posed and answered in this work:

- How much air flows through the crib under unrestricted quiescent ambient conditions? By comparing the burning rates under a range of flows to the burning rate in unrestricted quiescent conditions, the amount of air naturally induced into a crib while burning was deduced and was found to be best related to the vent area and the square root of the stick spacing ($A_v s^{1/2}$). It was seen that the air-to-fuel ratio inside a fuel bed burning in quiescent conditions is approximately 1.11, indicating that over 75% of the air required to completely combust the pyrolysis gases is entrained in the plume above.
- What happens when that flow is reduced? When the supplied air is less than the amount normally entrained in ambient burning, the crib is under-ventilated and the proportional reduction in the burning rate does not seem to depend on the crib characteristics and is controlled only by the access to air.
- What happens when that flow is increased? Do the characteristics of the crib change the behavior? When the crib is over-ventilated, the relative increase in the burning rate does vary with crib design. It was shown that if the non-dimensional factor $(b/\phi)^{0.25}$ was included when examining the variation in the burning rate per stick surface area (fuel mass flux) with the air flow rate per

stick surface area (air mass flux), the data generally collapse to a single curve. An examination of the air-to-fuel ratios also correlated the data reasonably well for just simple physical arguments.

Unfortunately, higher flow rates were not possible with the current setup but there is a need to test higher flows to examine the conditions under which the burning rate begins to decrease with air flow rate. In order to capture some of the more extreme fire behavior, future wildland fire models will need to include the interactions between the fire and the atmosphere [31] that can produce very strong local winds on the ground [23], separate from wind due to weather. Understanding when the wind is strong enough to reduce the burning rate could be a needed natural limiter in future wildland fire models to avoid “runaway” spread rates. Note that directly translating these imposed airflow rates to a relevant wind velocity requires some assumptions and calculations to determine how the flow penetrates the fuel bed, especially for surface fuels. Future work will need to include the effect of moisture content. The combustion efficiency in conditions ranging from under- to over-ventilated is important for understanding the emissions of wildland fires. Measurements should be made to examine the CO and CO₂ produced in the full range of ventilation conditions. Though wood cribs have been used to understand wildland fire behavior for quite some time [1], a concerted effort is still required to link relevant crib properties to realistically measurable properties of wildland fuels. Because wildland fuels are not composed entirely of homogenously sized fuel elements, cribs with mixed fuel element thicknesses are a logical next step to start bridging the gap to the more complex wildland fuel beds. Though this work is motivated by the need to better understand wildland fire behavior, care should be exercised when applying the findings of this work to the wildland fire context to carefully consider the boundary conditions used here (fuel raised above the ground with somewhat uniform flow throughout, axisymmetric plumes) compared to those of wildland fuels (typically in a line fire configuration).

Acknowledgements

The authors would like to thank Chelsea Phillips and Sophia Vernholm for the construction of the cribs; Cyle Wold for the data acquisition setup; Josh Deering for the construction of the apparatus; and Mark Finney for the many discussions.

Funding

Funding was provided by the National Fire Decision Support Center.

Declarations

Conflict of interest The authors declare that they have no conflict of interest.

Open Access

This article is licensed under a Creative Commons Attribution 4.0 International License, which permits use, sharing, adaptation, distribution and reproduction in any medium or format, as long as you give appropriate credit to the original author(s) and the source, provide a link to the Creative Commons licence, and indicate if changes were made. The images or other third party material in this article are included in the article's Creative Commons licence, unless indicated otherwise in a credit line to the material. If material is not included in the article's Creative Commons licence and your intended use is not permitted by statutory regulation or exceeds the permitted use, you will need to obtain permission directly from the copyright holder. To view a copy of this licence, visit <http://creativecommons.org/licenses/by/4.0/>.

References

1. Rothermel RC (1972) A mathematical model for predicting fire spread in wildland fuels. Research Paper INT-115, Intermountain Research Station, USDA Forest Service, p 40
2. Heinsch FA, Andrews PL (2010) BehavePlus fire modeling system, version 5.0: design and features. General Technical Report RMRS-GTR-249, Rocky Mountain Research Station, USDA Forest Service, p 111
3. Finney MA (1998, revised 2004) FARSITE: Fire Area Simulator-model development and evaluation, Res. Pap. RMRS-RP-4, Rocky Mountain Research Station, U.S. Department of Agriculture Forest Service, p 47
4. Fire Danger Group (1992) Development and structure of the Canadian Forest Fire Behavior Prediction System, vol 3. Forestry Canada, Science and Sustainable Development Directorate
5. Cruz MG, Gould JS, Alexander ME, Sullivan AL, McCaw WL, Matthews S (2015) A guide to the rate of fire spread models for Australian vegetation. Australasian Fire and Emergency Service Authorities Council Ltd. And Commonwealth Scientific and Industrial Research Organisation, Melbourne, p 123
6. Werth PA, Potter BE, Alexander ME, Clements CB, Cruz MG, Finney MA, Forthofer JM, Goodrick SL, Hoffman C, Jolly WM, McAllister SS, Ottmar RD, Parsons RA (2016) Synthesis of knowledge of extreme fire behavior: volume 2 for fire behavior specialists, researchers, and meteorologists. Gen. Tech. Rep. PNW-GTR-891. Portland, OR: U.S. Department of Agriculture, Forest Service, Pacific Northwest Research Station, p 258
7. Hiers JK, O'Brien JJ, Varner JM et al (2020) Prescribed fire science: the case for a refined research agenda. *Fire Ecol* 16:11
8. Finney MA, McAllister SS, Grumstrup TP, Forthofer JM (2021) Wildland fire behavior: dynamics, principles and processes. CSIRO Publishing, Clayton South, p. 360
9. Finney MA, Cohen JD, McAllister SS, Jolly WM (2012) On the need for a theory of wildland fire spread. *Int J Wildland Fire* 22:25–36
10. Thomas PH (1963) The size of flames from natural fires. *Symp (Int) Combust* 9:844–859
11. Fons WL, Clements HB, George PM (1963) Scale effects on propagation rate of laboratory crib fires. *Symp (Int) Combust* 9:860–866

12. Anderson HE (1990) Relationship of fuel size and spacing to combustion characteristics of laboratory fuel cribs. Research Paper INT-424, Intermountain Research Station, USDA Forest Service, p 12
13. Byram GM, Clements HB, Elliott ER, George PM (1963) An Experimental Study of Model Fires. Technical Report No.3, Southeastern Forest Experiment Station, Southern Forest Fire Laboratory, Macon, Georgia USDA Forest Service, p 36
14. Gross D (1962) Experiments on the burning of cross piles of wood. *J Res Natl Bureau Stand* 66c(2):99–105
15. Block JA (1971) A theoretical and experimental study of nonpropagating free-burning fires. *Symp (Int) Combust* 13:971–978
16. Heskestad G (1973) Modeling of enclosure fires. *Symp (Int) Combust* 14:1021–1030
17. Thomas PH (1973) Behavior of fires in enclosures – some recent progress. *Symp (Int) Combust* 14:1007–1020
18. McAllister S, Finney M (2016) Burning rates of wood cribs with implications for wildland fires. *Fire Technol* 52:1755–1777
19. Ingason H, Li YZ (2010) Model scale tunnel fire tests with longitudinal ventilation. *Fire Saf J* 45:371–384
20. Diab MT, Haelssig JB, Pegg MJ (2020) The burning behavior of wood crib fires under free burning and fire whirl conditions. *Fire Saf J* 112:102941
21. McAllister S, Finney M (2016) The effect of wind of burning rate of wood cribs. *Fire Technol* 52:1035–1050
22. McAllister S (2019) The role of fuel bed geometry and wind on the burning rate of porous fuels. *Front Mech Eng* 5:11. <https://doi.org/10.3389/fmech.2019.00011>
23. McAllister S (2021) Effect of reduced plume entrainment on the burning rate of porous fuel beds. *Prog Scale Model* 2(2):6. <https://doi.org/10.13023/psmij.2021.02-02-06>
24. McAllister S (2022) Burning rate and flow resistance through porous fuel beds: axisymmetric versus line fires. *Combust Sci Technol* . <https://doi.org/10.1080/00102202.2021.2019233>
25. Harmathy TZ (1976) The effect of ventilation on the burning of piles of solid fuels. *Combust Flame* 31(1):259–264
26. Evans DD, Emmons HW (1977) Combustion of wood charcoal. *Fire Saf J* 1(1):57–66
27. Harmathy TZ (1972) A new look at compartment fires, part 1. *Fire Technol* 8(3):196–217
28. Quintiere JG (2006) Fundamentals of fire phenomena. Wiley, West Sussex, pp. 318–322
29. Heskestad G (2006) Heat of combustion in spreading wood crib fires with application to ceiling jets. *Fire Saf J* 41(5):343–348
30. Quintiere JG, McCaffrey BJ (1980) The burning of wood and plastic cribs in an enclosure: Volume 1. NBSIR 80–2054, National Bureau of Standards, p 180
31. Potter BE (2002) A dynamics based view of atmosphere-fire interactions. *Int J Wildland Fire* 11:247–255